Light-responsive hybrids based on carbon nanotubes with covalently attached PHEMA-g-PCL brushes

Light-responsive hybrids based on carbon nanotubes with covalently attached PHEMA-*g*-PCL brushes

Katarína Mosnáčková[1]*, Miroslav Mrlík[2], Matej Mičušík[1], Angela Kleinová[1], Vlasta Sasinková[3], Anton Popelka[4], Alena Opálková Šišková[1], Peter Kasák[4,]*, Claudia L. Dworak[5], Jaroslav Mosnáček[1,6]*

[1]*Polymer Institute, Slovak Academy of Sciences, Dúbravská cesta 9, 845 41 Bratislava, Slovakia*

[2]*Centre of Polymer Systems, University Institute, Tomas Bata University in Zlin, trida Tomase Bati 5678, 760 01 Zlin, Czech Republic*

[3]*Institute of Chemistry, Slovak Academy of Sciences, Dúbravská cesta 9 845 38 Bratislava, Slovakia*

[4]*Center for Advanced Materials, Qatar University, Doha 2713, Qatar*

[5]*Institute of Applied Synthetic Chemistry, Vienna University of Technology, Getreidemarkt 9, A-1060 Vienna, Austria*

[6]*Centre for Advanced Materials Application, Slovak Academy of Sciences, Dubravska cesta 9, 845 11 Bratislava, Slovakia*

For Table of Contents use only

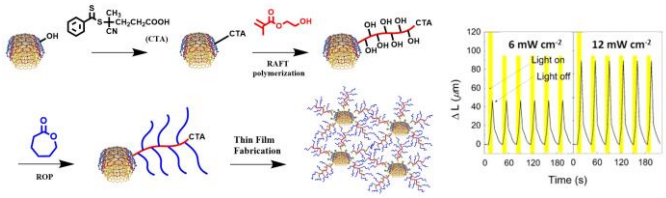

KEYWORDS: brush block copolymers, grafting from surface, reversible deactivation radical polymerization, surface-initiated polymerization, thermoplastic elastomers.

ABSTRACT

Carbon nanotube (CNT)-based materials allow for the direct conversion of light into heat and then into mechanical force in so-called photo-mechanical effect. This effect has been observed almost solely in the form of polymer (nano)composites, where CNTs act as active fillers. To overcome the issue with heterogeneous distribution, hybrids based on multiwalled carbon nanotubes (MWCNTs), covalently modified with poly(2-hydroxyethyl methacrylate)-*graft*-poly(ε-caprolactone) brushes (MWCNTs-PHEMA-*g*-PCL), were prepared, and their photo-mechanical actuator behavior, without the need for mixing with an elastomer, was proven. The MWCNT-PHEMA-*g*-PCL hybrids were synthesized using the surface-initiated reversible addition-fragmentation chain transfer polymerization of 2-hydroxyethyl methacrylate, with subsequent ring-opening polymerization of ε-caprolactone from the pendant hydroxyl groups of PHEMA. It was found that the MWCNT-PHEMA-*g*-PCL hybrid material containing 24 wt% of MWCNTs possesses the properties of thermoplastic elastomers, while retaining their elastic properties at least up to 100 °C. It exhibits an excellent, fully reversible, repeatable, and fast photo-mechanical actuation behavior.

INTRODUCTION

Since their discovery by Iijima in 1991, carbon nanotubes (CNTs) have become an attractive material for many applications due to their unique properties, which make them applicable in the fields of nanoscience, bioengineering, and nanotechnology [1]. The main obstacles to their use in many applications are their chemical inertness and hydrophobicity, resulting in a low solubility/dispersivity in most solvents [2]. Moreover, CNTs tend to agglomerate due to their large aspect ratios and the strong π-π interactions between them, resulting in a problematic dispersibility in solvents and polymer matrices [3,4]. The agglomeration can be avoided by chemical functionalization. The functionalization can provide an improvement of the dispersibility of the prepared hybrid fillers, ensure their exfoliation in polymer bulk, as well as improve their compatibility with other components [5]. The functionalization of CNTs by polymer chains is usually performed after the initial modification of CNTs, either via oxidation [6–10] or diazonium coupling reactions of aniline derivatives in the presence of alkyl nitrite [11–14]. Oxidation is one of the most widely used methods for CNT sidewall modification. The main feature of this type of functionalization is that only a small fraction of the carbon in the nanotube becomes functionalized, usually ranging from 0.25 to 3.5 wt.% [6]. In contrast to the oxidation approach, the diazonium coupling approach provides the anchoring of chemical moieties bearing different functional groups (COOH, OH, NH_2, COCl, COOEt, NO_2, Cl, and F) at a high functionalization degree (up to 21 wt.% [13]), which allows for the use of a broad range of grafting polymerization techniques [11,13,15].

Nowadays, controlled polymerization techniques are widely used for the surface modification of CNTs. The "grafting from" approach results in polymer coatings with a precisely controlled structure and architecture of the grafted polymer chains, with the possibility of varying the grafting density [15,16]. Reversible deactivation radical polymerization (RDRP) techniques are characterized by a good control over the molecular characteristics, with

negligible both chain transfer and irreversible termination [17]. Reversible addition-fragmentation chain transfer (RAFT) polymerization is one of the RDRP techniques and is highly adaptable and widely applicable for various vinyl monomers with a wide range of both solvents and reaction temperatures [18]. RAFT is based on degenerative chain transfer reactions, which are usually mediated by a thiocarbonylthio-based chain transfer agent (CTA) [19]. General strategies for surface-initiated RAFT polymerization (SI-RAFT) can be achieved in two different ways: (a) covalent anchoring of a free radical azo-initiator to the surface, followed by SI-RAFT polymerization in the presence of a CTA in the solution [20–22]; (b) surface CTA attachment, followed by SI-RAFT, which is initiated by a free radical azo-initiator [7,9,10,16,23–29].

Both neat CNTs [30] and polymer-coated CNT hybrids [31] were also studied in relation to their application as photo-mechanical actuators. Photo-mechanical actuators belong to the group of smart materials that change their physical properties in the presence of a light stimulus [32]. Since the neat CNTs showed a limited capability, and their dispersion seems to be crucial [30], modification techniques were used to improve this. Non-covalent modification was effectively applied to improve the dispersion and thus the photo-mechanical actuation capability [33]. However, this is just a short-term solution due to the fact that the migration of the non-covalently attached moieties can occur. Therefore, Ilčíková et al. showed that the covalent modification of CNTs with polymers of a similar structure as that of polymer matrices (polystyrene-based [34] and poly(methyl methacrylate)-based thermoplastic elastomers [35]) can lead to a significantly improved photo-actuation capability and also to a long-term overall mechanical stability of the composite. It was found that the important factors affecting the photo-mechanical actuation performance are the homogeneous distribution of the CNTs within the polymer matrix and the retention of the elastic properties at higher temperatures.

Therefore, here, we decided to investigate the photo-mechanical actuation performance of neat hybrids consisting of MWCNTs with a covalently bound poly(2-hydroxyethyl

methacrylate)-*graft*-poly(ε-caprolactone) (PHEMA-*g*-PCL) brush copolymer. In such a material, the homogeneous covering of the MWCNTs by polymers should ensure the homogeneous distribution of MWCNTs within the material. At the same time, a sufficiently high content of PCL polymer with a low T_g and relatively low T_m could, under irradiation, provide the material with elastic behavior, in which CNTs will also serve as crosslinking points at higher temperatures. Thus, the work presented here demonstrates the preparation of novel hybrids based on MWCNTs modified through the "grafting from" strategy by the combination of the RAFT polymerization of HEMA and, subsequently, the ring-opening polymerization (ROP) of ε-caprolactone CL, initiated by the pendant hydroxyl of PHEMA chains. The particular synthetic step and the final MWCNT-PHEMA-*g*-PCL hybrid were analyzed using numerous experimental techniques, while MWCNT-PHEMA-*g*-PCL showed a fully reversible and fast photo-mechanical actuation performance in a repeatable manner within the tested number of 11 consecutive light off–on cycles.

EXPERIMENTAL

Materials

Multiwalled carbon nanotubes (MWCNTs) were provided by Nanostructured & Amorphous Materials (Houston, TX). The MWCNTs were obtained using a chemical vapor deposition, with an outside diameter of 60-100 nm, length of 5-15 μm, specific surface area of 40-600m^2/g, and purity > 95%. 4-(4-cyanopentanoic acid) dithiobezoate (CPAD) (Sigma Aldrich, > 97%) and 2-hydroxyethyl methacrylate (HEMA) were purchased from Acros Organics, with a purity > 98%. Azobisisobutyronitrile (AIBN) (Sigma Aldrich, ≥ 98%) was purified by recrystallization from ethanol. *N*,*N*-Dimethylformamide (DMF) was supplied by Acros Organics, with a purity of 99.8%. ε-Caprolactone (ε-CL, Sigma Aldrich, 97%) was distilled twice before use. Stannous octoate ($SnOct_2$) was received from Sigma Aldrich with

purity 92.5 – 100.0%. Ethylene glycol (anhydrous, 99.8%) and thionyl chloride (97%) were supplied by Sigma Aldrich, and 4-dimethylaminopyridine (DMAP, 99%) and *N,N′*-dicyclohexylcarbodiimide (DCC, 99%) were obtained from Acros Organics and were used directly. All other reagents were used without further purification.

Analyses

The ^{1}H NMR spectra were recorded on a Bruker Avance 400 MHz spectrometer, using deuterated methanol or chloroform as a solvent.

The molar masses and molar masses dispersity were determined using gel permeation chromatography (GPC), consisting of a P102 pump from Watrex, with a flow rate of 1.0 mL/min, and evaporative light scattering detector (ELSD) model 1000 from PL-Agilent UK-USA at an evaporation temperature of 120 °C. As a stationary phase, the column TSKgel GMH_{HR} -M from TOSOH was used. The DMF from Sigma-Aldrich or chloroform from MACRON, both HPLC grade, was used as an eluent. The GPC system was calibrated with polystyrene standards.

The ATR-FTIR spectroscopy measurements were performed using a Nicolet Impact 400 FTIR spectrometer, with a resolution of 4 cm^{-1} and a scan range of 4000 – 400 cm^{-1}. Raman measurements were performed using a Thermo Fisher Scientific DXR Raman microscope, with a 532 nm laser.

The XPS spectra were recorded using a Thermo Scientific K-Alpha XPS system (Thermo Fisher Scientific, UK), equipped with a monochromatic Al Kα X-ray source (1486.68 eV). An X-ray beam of 400 μm was used at 6 mA × 12 kV. The spectra were acquired in the constant analyzer energy mode, with a pass energy of 200 eV, for the survey. Narrow regions were collected with a pass energy of 20 eV. The Thermo Scientific *Avantage* software, version 5.9918 (Thermo Fisher Scientific Inc., East Grinstead, UK), was used for digital acquisition

and data processing. Spectral calibration was achieved using the automated calibration routine and the internal Au, Ag, and Cu standards supplied with the K-Alpha system.

The X-ray diffraction spectra were taken on Empyrean (PANalytical) diffractometer using the irradiation source, Cu Kα1 (0.15406 nm), at a tension of 45 kV, current of 40 mA, and the PIXcel1D detector. The data were acquired in gonio mode within a 2θ range from 10° to 60°, with a step size of 0.0066° and scan speed of 0.01° s^{-1}. The Debye–Scherrer equation is as follows [36].

$$D = 0.94\frac{\lambda}{\beta cos\theta} \qquad (1)$$

where D is the apparent particle size, *â* is the full-width at half-maximum (FWHM) of the X-ray diffraction line in radians, ë is the wavelength (0.15425 nm), and č is the angle between the incident ray and the scattering planes.

Thermogravimetric analysis (TGA) was conducted using the TGA instrument Perkin Elmer TGA 4000 (PerkinElmer, USA) under a flow of nitrogen atmosphere and at a temperature range from 50 °C to 700 °C and heating rate of 10 °C min^{-1}.

Broad dielectric spectrometry was carried out on a Broadband Dielectric Impedance Analyzer (Novocontrol, Germany) in the frequency range from 0.01 Hz to 10 MHz, and the standard sample cell BDCS 140 was used.

The surface morphologies of the MWCNT hybrids were analyzed using an optical surface metrology confocal system profilometer, Leica DCM8 (Leica Microsystems, Germany). The images, with a surface area of approximately 29 × 22 μm^2, were obtained using a 100 × magnification objective, with 6x zooming and EPI 100X 0.9-L objective lens.

The surface morphologies/topographies of the MWCNT hybrids were observed by atomic force microscopy (AFM) using an MFP-3D system (Asylum Research, USA), equipped with an AC160TS cantilever (Al reflex coated Veeco model-OLTESPA, Olympus, Japan). Scanning

was carried out under ambient conditions using tapping mode in air (AC mode) at a scan rate of 0.5 Hz over an area of 5 × 5 μm^2.

The dynamic mechanical analysis was performed using DMA/SDTA 861 (Mettler Toledo, Switzerland) in shear mode at a frequency of 1 Hz in a temperature range from 25 °C to 100 °C and under a nitrogen atmosphere. The linear viscoelastic region (LVR) was established from Fig. 9a at 0.1 strain deformation (γ) value. Frequency sweeping was performed in the LVR from 0.05 Hz to 50 Hz. The samples of a circular shape with an 8 mm diameter and 0.3 mm thickness were cut from the films prepared by the solution casting method, using chloroform as a solvent.

The photo-mechanical actuation performance of the samples were measured using thermo-mechanical analyzer (TMA, Mettler Toledo) following previously reported studies for comparison [31]. Briefly, a red LED diode (Luxeon Rebell, Philips) was applied for irradiation, and 10 s on/ 50 s off intervals were established. The diode operates at 627 nm at various light source intensities from 6 mW to 12 mW, under a 7% pre-strain of the samples. The investigated samples were in the form of stripes, with a 15 mm length, 1.9 mm width, and 0.3 mm thickness.

Preparation of MWCNTs-OH

A suspension of MWCNTs (2.0 g) in 65% nitric acid was prepared by bath sonication for 30 min and subsequent stirring under reflux for 24 h. After cooling them down to laboratory temperature, the carboxylated MWCNTs were separated by vacuum filtration and washed with deionized water several times, until a neutral pH was achieved. The isolated product was dried under vacuum at 50 °C, yielding 1.22 g of MWCNTs-COOH. Dried MWCNTs-COOH (1.2 g) were reacted with a $SOCl_2$ excess (50 mL) under reflux for 24 h. The residual $SOCl_2$ was removed under vacuum. The remaining MWCNTs-COCl were immediately reacted, without further purification, with ethylene glycol (40 mL) at 120 °C for 24 h. The solid product was separated by vacuum filtration using a 0.22 μm PTFE membrane and carefully washed out with

deionized water and THF. The resultant solid was dried overnight under vacuum at 50 °C, yielding 1.0 g of hydroxyl group-functionalized MWCNTs (MWCNTs-OH).

Attachment of CPAD on the MWCNT surfaces

The compounds CPAD (0.63 mmol, 177 mg) and MWCNTs-OH (0.60 g), were added to a 25 mL two-necked flask, and the mixture was sonicated in 10 mL of DMF for 30 min. After the addition of DMAP (75 mg) and DCC (130 mg) to the mixture, the dispersion of MWCNTs-OH was reacted for 1 h at 0 °C. Subsequently, the mixture was stirred at room temperature in the dark for 48 h. Then, the solid part was filtered off using a 0.22 μm PTFE membrane and washed out with ethanol, THF, and deionized water to completely remove any possible absorbed CPAD. The resultant solid was dried overnight under vacuum at room temperature, yielding 0.50 g of MWCNTs-CPAD.

Grafting of poly(2-hydroxyethyl methacrylate) via surface-initiated RAFT polymerization

100 mg of MWCNTs-CPAD, HEMA (1.65 g, 12.6 mmol), free CPAD (9 mg, 0.03 mmol), and 4 mL of DMF were added to a 10 mL dry Schlenk flask and sealed with a glass stopper. After sonication for 30 min at 25 °C, the Schlenk flask was degassed by three freeze-pump-thaw cycles, back filled with argon, immersed in an oil bath pre-heated to 70 °C, and stirred. Polymerization was initiated by the addition of 0.127 mL of azo-initiator (AIBN) from a stock solution of 0.5 M AIBN in DMF. The polymerization was quenched after 24 hours by the immersion of the flask in ice water, and the polymerization mixture was diluted with 200 mL of DMF, sonicated for 30 min at 25 °C, and filtered through a 0.22 μm polycarbonate membrane. To ensure that free polymer chains were completely removed from the product, it was subsequently purified by dispersion in methanol and filtering. This procedure was repeated three times, followed by drying under vacuum to a constant weight.

Cleavage of poly(2-hydroxyethyl methacrylate) from MWCNTs-PHEMA

PHEMA chains were cleaved from the MWCNT surfaces under basic conditions as follows: The MWCNTs-PHEMA (50 mg) was dispersed in 50 mL of a solution prepared from 1 M NaOH and ethanol (1:1) and stirred under reflux for 48 h. The reaction mixture was then filtered through a 0.22 μm polycarbonate membrane. The resultant MWCNTs, after PHEMA cleavage, were analyzed by Raman spectroscopy.

Synthesis of MWCNTs-PHEMA-g-PCL hybrids

The resulting MWCNTs-PHEMA (80 mg), ε-CL (2.4 g, 0.021 mol), and $SnOct_2$ (1.05×10^{-4} mol) were placed in a two-necked flask and sonicated for 30 min at 25 °C. The bulk polymerization was carried out in an inert atmosphere under reflux for 4 h at 140 °C. The polymerization was stopped by cooling down to room temperature, 200 mL of CH_2Cl_2 was added, and the mixture was filtered through a 0.22 μm PTFE membrane. The solid was thrice re-dissolved in a mixture of CH_2Cl_2:acetonitrile (1:2 by volume) and separated by centrifugation at 20 000 rpm for 15 min. The MWCNT-PHEMA-*g*-PCL hybrids were dried under vacuum at 60 °C for 24 h. The non-grafted PCL, formed from the water present in the system, was precipitated from the collected solutions into the methanol, dried under vacuum, and analyzed by GPC (see Fig S2).

Synthesis of MWCNT-PCL hybrids

The MWCNTs-OH (80 mg), ε-CL (2.4 g, 0.021 mol), and $SnOct_2$ (1.05×10^{-4} mol) were placed in a two-necked flask, purged with argon for 15 min, and sonicated for 30 min at 25 °C. The polymerization was carried out at 140 °C for 2 h and stopped by cooling down to room temperature and adding 200 mL of CH_2Cl_2. The mixture was filtered through a 0.22 μm PTFE

membrane, and the solid was thrice re-dissolved in a mixture of CH_2Cl_2:acetonitrile (1:2 by volume) and separated by centrifugation at 20 000 rpm for 15 min. The MWCNT-PCL product was dried under vacuum at 60 °C for 24 h. The non-grafted PCL, formed from the water present in the system, was precipitated from the collected solutions into the methanol and analyzed by GPC.

Synthesis of PHEMA-g-PCL matrix

HEMA (0.165 g, 1.26 mmol), free CPAD (2.5 mg, 0.008 mmol), and 2 mL of DMF were added to a 10 mL dry Schlenk flask and sealed with a glass stopper. The Schlenk flask was degassed by three freeze-pump-thaw cycles, back filled with argon, immersed in an oil bath pre-heated to 70 °C, and stirred for 24 hours. Polymerization was initiated by the addition of AIBN (6×10^{-4} mmol from stock solution of 0.5 M AIBN in DMF). The polymerization was stopped after 24 hours by the immersion of the flask in ice water and aeration. The monomer conversion determined by ^{1}H NMR was 82%. The M_n and dispersity of PHEMA were 11,000 g mol^{-1} and 1.26, respectively.

PHEMA (0.135 g, 1.04 mmol of hydroxyl groups) in 1.5 mL of DMF, ε-CL (9.9 g, 86.6 mmol), and $SnOct_2$ (352 mg, 0.86 mmol) were placed in a two-necked flask and purged with argon for 15 minutes. The polymerization was carried out at 140 °C and stopped after 4 h by cooling down to room temperature. Subsequently, 200 mL of CH_2Cl_2 was added, and the mixture was precipitated twice into the methanol dried under vacuum. The bimodal character of GPC traces was observed with the M_n of individual peaks of 139,000 g mol^{-1} and 3400 g mol^{-1}, corresponding to the PHEMA-*g*-PCL copolymer and PCL homopolymer, respectively, at an approximate ratio of 2:1 (see Fig S3).

RESULT AND DISCUSSION

Synthesis design

The overall synthesis route for preparation of novel hybrid material based on MWCNTs grafted with brush copolymer is presented in Figure 1. It is well known that MWCNTs possess light-to-heat-to-mechanic conversion activity, where they serve as a light absorber and molecular heater at the same time. Such properties were used primarily in composite materials to form actuator or storage material [37]. The advantage and significance of the hybrid designed in the present work is that it does not need to use any polymer matrices or other components for its photo-mechanical actuation performance. Rationally, the oxidation of MWCNTs to form MWCNTs-COOH (Figure 1, step A-1) was chosen as a technique for introducing a low population of reactive places, allowing for subsequent brush-like structure formation. The subsequent reaction with ethylene glycol allowed for the introduction of hydroxyl groups (MWCNTs-OH, Figure 1, steps A-2 and A-3) for further modification. The CPAD was used as a CTA for covalent bonding on the MWCNT-OH (Figure 1, step B). Dithiobenzoates are frequently used as CTAs for the RAFT of (meth)acrylate and styrene-based monomers [38–40]. Moreover, they are utilized for the grafting of polymers from a wide range of surfaces, such as silica and gold nanoparticles [16,41], cellulose [42], and MWCNTs [10]. The surface immobilization of CPAD to MWCNTs-CPAD was conducted using the R-group approach through a condensation reaction between carboxyl functional groups of CPAD and hydroxyl groups present on the MWCNT-OH surfaces. Further, MWCNTs-CPAD were grafted with PHEMA using SI-RAFT polymerization to MWCNTs-PHEMA in order to increase the population of hydroxyls, as pendant groups. (Figure 1, step C). Finally, the pendant hydroxyl groups of PHEMA were used as initiators for the ROP of ε-CL to produce MWCNTs-HEMA-*g*-PCL (Figure 1, step D).

From the point of view of the applicability of such a material, it is worth mentioning that in addition to the expected photo-mechanical actuation behavior, the poly(hydroxyethyl

methacrylate)-*graft*-poly(ε-caprolactone) (PHEMA-*g*-PCL) grafted to the different types of surface, such as hydroxyapatite [25], silicon wafer [43], Fe_3O_4 magnetic nanoparticles [44], and carbon black [45], has previously been found to improve the physicochemical and thermoresponsive properties, and thanks to the biocompatible and hydrophobic characters of PCL, the hybrids can also be used for various biomedical applications [46,47].

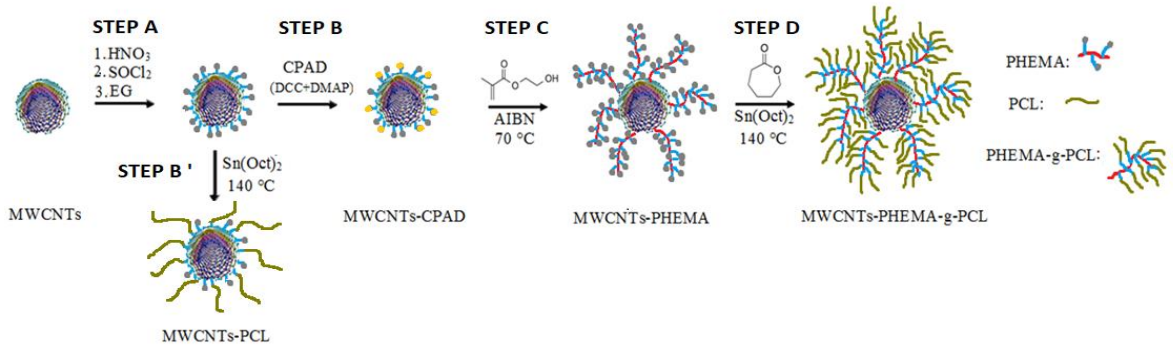

Figure 1. Schematic illustration of the sequential grafting of polymers from the surface of the MWCNTs.

PCL, HEMA-*g*-PCL, and MWCNTs-PCL (Figure 1 step B') were also prepared and included in the discussion to compare them with the properties of the MWCNT-HEMA-*g*-PCL hybrid.

Synthesis and characterization of MWCNTs-PHEMA-g-PCL

The successful incorporation of CPAD on the surface was verified using ATR-FTIR and XPS. The FTIR spectra (Figure S4a) of MWCNTs-OH showed the absorption of OH groups at around 3280 cm^{-1}. After the subsequent attachment of CPAD, the absorption peak at 1086 cm^{-1} assigned to the vibration of the C=S group [26] appeared. Additional characteristic peaks of CTA moieties, such as C-H and C=O stretching vibrations centered at 2920 and 1720 cm^{-1}, respectively, could also be seen (Figure S4b). The modification of the surface of the MWCNTs

was also confirmed by XPS analysis (Table 1 and Figure 2). Pure MWCNTs showed only a small oxidation on the surface, with a strong C1s asymmetric signal from sp^2 carbon at ~ 284.4 eV and a symmetric loss peak at 291 eV, corresponding to excited π electrons (labeled as π-π* in Figure S5). The MWCNT-OH sample showed a signal increase at ~ 286.0 eV, corresponding to the C-O group [48]. Additionally, an increase of oxygen signals, corresponding to aromatic carbonyls ($C=O_{ar}$ at ~531.5 eV), aliphatic carbonyls ($C=O_{al}$ at ~532.4 eV), and hydroxyls (C-O at ~533.4 eV), was observed. In the XPS spectra of MWCNTs-CPAD, a successful immobilization of CTA on the MWCNT-OH surfaces was confirmed by presence of sulphur and nitrogen elements at ~ 164.1 eV and ~ 399.5 eV, respectively, due to the CPAD modification (Figure 2b, Table 1). [10]

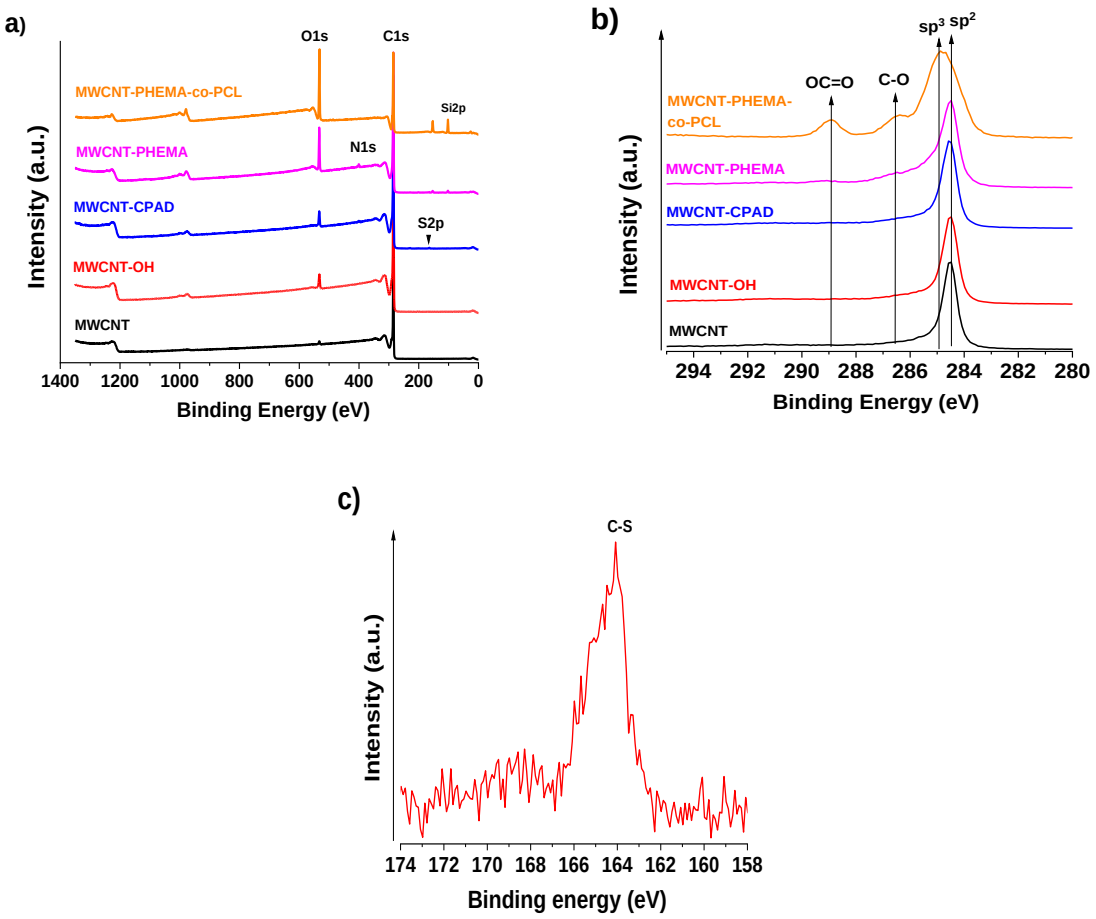

Figure 2. XPS data of a) neat and modified MWCNTs, b) C1s comparison of neat and modified MWCNTs, and c) S2p region of MWCNT-CPAD.

Table 1. Surface composition of the samples in atomic percentages, as determined from the XPS survey spectra.

	Surface chemical composition (at.%)			
Sample	O1s $C=O_{ar}/C=O_{al}/C-O$/#	C1s sp^2/sp^3/CO/C=O/OCO/*	S2p	Cl2p/ N1s/Si2p/Sn3d
MWCNTs	1.2 0.1/0.6/0.4/0.1	98.8 89.6/5.3/1.2/-/-/2.8	-	-/-/-
MWCNTs-OH	4.3 1.4/1.1/1.5/0.3	95.5 83.6/6.6/2.3/-/0.1/3.0	0.1	0.1/-/-
MWCNTs-CPAD	4.5 0.5/1.7/2.1/0.2	94.7 76.8/9.3/4.7/-/0.7/3.1	0.3	0.1/0.4/-
MWCNTs-PHEMA	11.6 0.3/6.1/4.9/0.3	85.2 57.6/14.8/7.4/2.6/1.4/1.3	0.2	0.1/1.7/ 1.2
MWCNTs-PHEMA-g-PCL	23.6 0.6/15.4/7.1/0.5	66.9 8.5/40.5/10.2/1.4/6.2/0.1	-	-/-/9.3/0.1

refers to the O2C=O signal;[49] * refers to π-π* signal.

From the TGA curves (Figure 3), it can be seen that while crude MWCNTs remained basically stable up to 600 °C, MWCNTs-OH had about a 2.5% weight loss below 450 °C, and MWCNTs-CPAD had about a 4.0% weight loss below 450 °C. The weight loss difference of 1.5% for MWCNTs-CPAD corresponds to a CPAD concentration of 5.5×10^{-5} mol per gram of MWCNTs-CPAD.

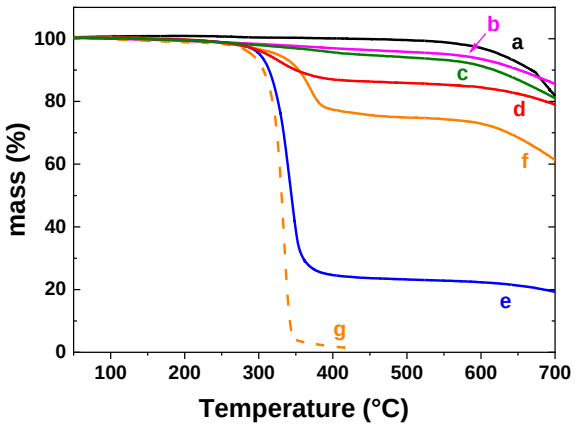

Figure 3. TGA curves of (**a**) crude MWCNTs, (**b**) MWCNTs-OH, (**c**) MWCNTs-CPAD, (**d**) MWCNTs-PHEMA, (**e**) MWCNTs-PHEMA-*g*-PCL, (**f**) MWCNTs-PCL, and (**g**) PCL.

The MWCNTs-CPAD were used for the RAFT polymerization of HEMA. In order to suppress the termination reactions on the surface due to the high local concentration of radicals, sacrificial CTA was also used. Free CTA is commonly added to a reaction system to suppress termination reactions by recombination and to improve the control of the growth of molar masses of the grafted polymers [27–29,50–52]. After 24 hours of polymerization, MWCNTs-PHEMA was separated from the free PHEMA formed from the sacrificial CTA. The M_n and dispersity of the free PHEMA were determined to be 12,300 g/mol and 1.2, respectively, confirming a good control of the polymerization. The chemical structure of the polymers grafted onto the MWCNT surfaces was confirmed by FTIR and XPS. In the FTIR spectra of MWCNTs-PHEMA, the peak at 3425 cm^{-1} can be attributed to the stretching vibration of the pendant hydroxyl groups of PHEMA (Figure 2). The presence of grafted PHEMA via the RAFT polymerization of HEMA was also proved by XPS, where a significant increase of the oxygen content, from 4.5 at.% for MWCNT-CPAD to 11.6 at.% for MWCNT-PHEMA, with an increase of the typical C1s signals at ~ 286.3 eV (C-O) and at ~ 289.0 eV (OC=O), was observed (Figure 2, Table 1). The signal of sp^2 carbon is a strong indication that the thickness of the PHEMA layer on the MWCNT surface is low.

The TGA of the MWCNTs-PHEMA showed a 10.5% weight loss in the region up to 450 °C (Figure 3). Thus, the density of the grafted PHEMA calculated from the TGA and M_n of PHEMA was ~ 1.2×10^{-2} chains per nm^2. This is in good agreement with our expectations, based on generally known lower density of functional groups obtained by the oxidation of CNTs, compared to the density of hydroxyl groups achieved by the modification of MWCNTs using diazonium chemistry[11]. In addition, the grafting density value is also in good agreement with a comparable "grafting from" experiment that we conducted using the ring-opening polymerization of CL from MWCNTs-OH. In this case, the weight loss in the TGA of the

MWCNTs-PCL was 24%, corresponding to the density of the grafted PCL, with an M_n of 49,700 g/mol and approximately 1.1×10^{-2} chains per nm^2.

The low grafting density determined for MWCNTs-PHEMA provided sufficient space for the subsequent grafting of the CL from the pendant hydroxyl groups of grafted PHEMA. After the grafting of PCL, the peak at 3425 cm^{-1} from the pendant hydroxyl groups of PHEMA was significantly decreased. At the same time, a significant increase of the absorption peaks at 1723 cm^{-1} and 2950 cm^{-1} from the carbonyl group stretching vibrations and C-H vibrations of the methylene groups, respectively, both attributed to PCL, were observed (Figure 4), similarly as reported by Lee et al.[53], and also observed by us, for MWCNTs directly grafted by PCL (see also Figure S6).

In XPS, the grafting of PCL from MWCNT-PHEMA resulted in a further increase of the oxygen content to 23.6 at.%. The C/O ratio for this sample was calculated to be ~ 2.84, which is close to the theoretical C/O ratio of pure PCL (equal to 3). It should be mentioned that, in the MWCNT-PHEMA-*g*-PCL sample, some silicon contamination (Si2p at ~ 102 eV) was also detected, so some of the determined oxygen can come from this contamination too, thus slightly increasing the C/O ratio. The C1s spectra showed a decrease of sp^2 carbon down to only 8.5 at.%, accompanied by the presence of strong C1s signals at ~ 286.3 eV (C-O) and at ~ 289.0 eV (OC=O), which is typical for polymers and indicates a dense coverage of the MWCNT surfaces by PHEMA-*g*-PCL copolymer (Figure 2, Table 1).

The TGA of MWCNTs-PHEMA-*g*-PCL showed a 76% weight loss. From the TGA results, it could be calculated that there is approximately 46 CL units per one HEMA unit grafted on the MWCNT surfaces. Thus, the average M_n of grafted PCL should be 5250 g/mol, under expectation that the ROP of CL was initiated from all hydroxyl groups of the grafted PHEMA. However, it should be pointed out that the M_n of free PCL formed simultaneously in the polymerization mixture, most probably initiated by residual water, which was found to be 22

600 g/mol. This inconsistency with the results from the TGA can be caused by steric hinderance in the case of a growth of PCL from MWCNTs-PHEMA, leading either to the formation of shorter grafted PCL chains, compared to the free ones, or a growth of PCL chains from not all hydroxyl groups of PHEMA or a combination of both, leading to the formation of a tree-shaped copolymer.

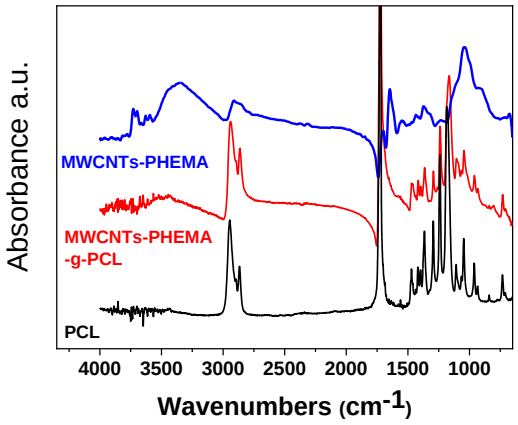

Figure 4. FTIR spectra of MWCNTs-PHEMA, MWCNTs-PHEMA-*g*-PCL, and PCL.

Raman spectroscopy provided additional proof of the sidewall functionalization of the MWCNTs. For the neat MWCNT sample, the strong peak at 1580 cm^{-1}, known as the G band, represents a high-frequency scattering mode of sp^2 hybridized carbon atoms bonded in a two-dimensional hexagonal lattice in a similar way to the vibration in a graphitic layer [54]. A disordered structure induced a peak in the region around 1350 cm^{-1} related to the D band, which is usually associated with the presence of defects in the hexagonal graphitic lattice. These defects correspond to the sp^3 carbon hybridization and usually serve as proof of the disruption of the conjugated delocalized π-electron system on the nanotube sidewalls. The increase in the sp^3 carbon population of the outer layer of the MWCNT surface may also be due to the covalently attaching functional groups and grafting with polymer chains [55–57]. Accordingly, the functionalization of MWCNTs significantly influenced the D-band intensity, resulting in a

gradual increase of the I_D/I_G ratio, with individual modification steps (Figure 5, Figure S8). The I_D/I_G ratio for MWCNTs-PHEMA and MWCNTs-PHEMA-*g*-PCL achieved values of 0.93 and 1.10, respectively, compared to the I_D/I_G ratio of 0.59 for neat MWCNTs. It is worth noting that, after the cleavage of the PHEMA chains from the MWCNT-PHEMA surface, the intensity of the D band significantly decreased, and the calculated I_D/I_G ratio was close to that determined for MWCNTs-OH (Figure S8). This confirmed that the changes in the I_D/I_G ratios were due to the modification of the surface by polymer chains.

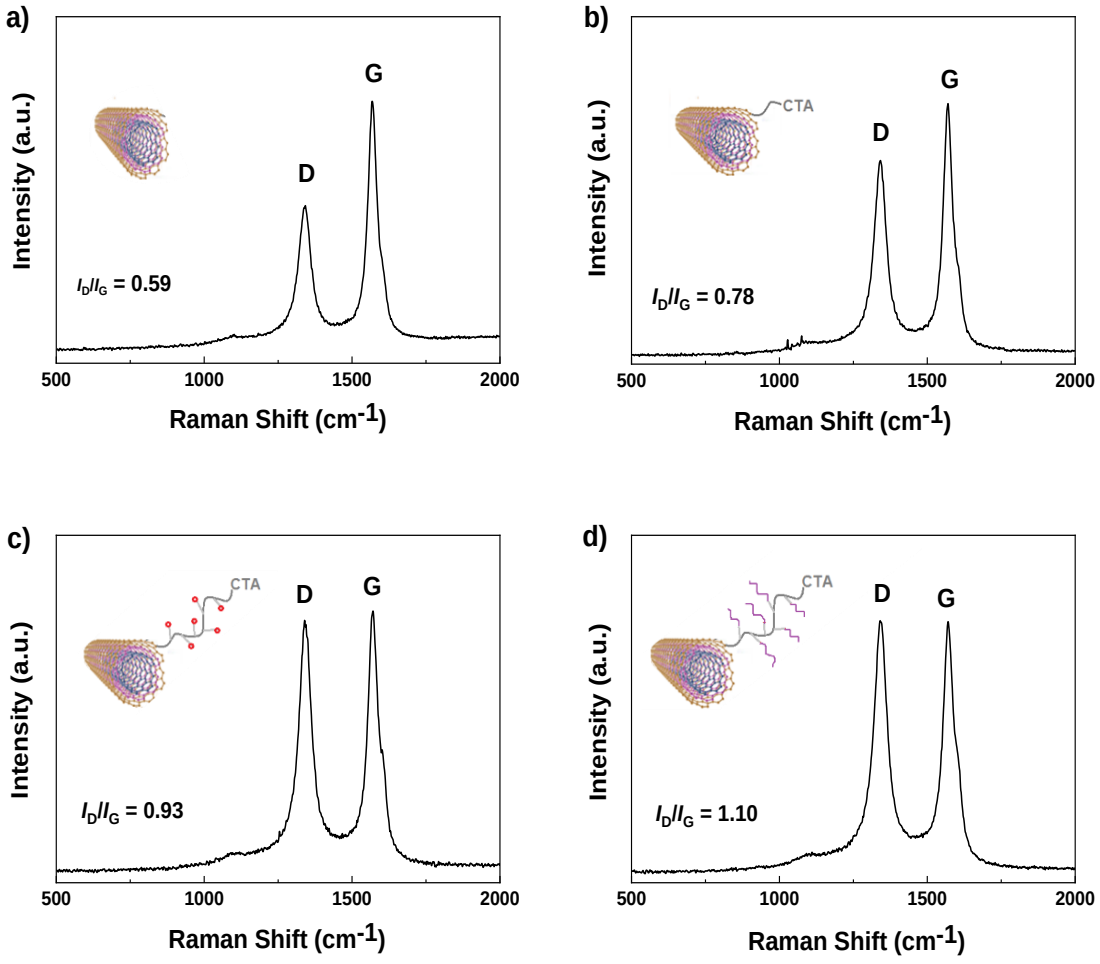

Figure 5. Raman spectra of (**a**) neat MWCNTs, (**b**) MWCNTs-CPAD, (**c**) MWCNTs-PHEMA, and (**d**) MWCNTs-PHEMA-*g*-PCL.

Physical structure

The physical structure of the MWCNTs-PHEMA-*g*-PCL was investigated using X-ray diffraction and DSC and compared with the structure of pure PCL, MWCNTs-PCL, and PHEMA-*g*-PCL. In the XRD profiles, the characteristic peaks of MWCNTs can be seen at the 2θ values of 26.4° and 43.40° indexed to the (002) and (100) reflection of the planes [58]. The inter-planar spacing (d) was calculated using Bragg's law ($n\lambda = 2d\sin\theta$), with a peak (002) at 0.331 nm. The modification of MWCNTs using the RAFT agent and grafting of MWCNTs with PHEMA did not influence the MWCNTs crystallographic structure. In sample MWCNTs-PHEMA, the amorphous structure of PHEMA was confirmed (Figure S10 and Figure 6). In the case of the MWCNT-PHEMA-*g*-PCL sample, the diffraction pattern shows characteristic PCL peaks at $2\theta = 21.3°$ and 23.6°, which correspond to the (110) and (200) crystallographic planes, respectively (Figure S11). Similarly, these peaks were also observable for the PCL, MWCNTs-PCL, and PHEMA-*g*-PCL samples (Figure 6, Figure S11). The apparent crystal size was obtained from FWHM by applying Equation (1) to the main peak (110). The results are summarized in Table 2. It can be seen that larger crystal domains were formed when PCL was grafted from either MWCNTs-OH or PHEMA, compared to neat PCL. In such cases, the crystallization of PCL can be simplified by the close presence of parallel PCL chains, thus simplifying the formation of larger crystal domains. On the other hand, smaller crystal domains were formed in the case of MWCNT-PHEMA-*g*-PCL. Even though in this hybrid the PCL chains are also grown close to each other, the limited space between the PHEMA grafts, in which the PCL chains are grown, provides steric hinderance. The steric hinderance can limit the PCL chain mobility and can result in a smaller crystal formation, even though the overall crystallinity does not need to be affected (see below).

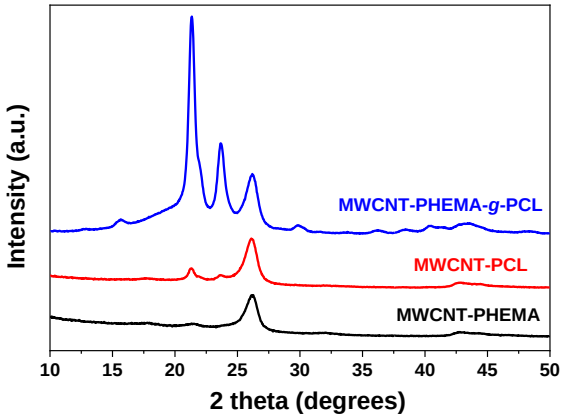

Figure 6. The XRD pattern of MWCNTs grafted with various polymers.

Table 2. Summary of the results from XRD analysis, determined from the peak corresponding to the (110) crystallographic plane, and from DSC analysis.

Sample	XRD			DSC			
	2θ [°]	FWHM [°]	D [Å]	T_c [°C]	T_m[a] [°C]	ΔH_m[a] [J/g]	X_c[a] [%]
PCL	21.36	0.606	139.5	28.1	54.7	64.4	47.3
MWCNT-PCL	21.32	0.582	145.2	42.0	52.4	30.5[b]	22.4
PHEMA-*g*-PCL	21.45	0.577	146.5	15.3	45.2	58.6	43.1
MWCNT-PHEMA-*g*-PCL	21.35	0.704	120.0	34.5	57.3	55.7[b]	40.9

[a] determined from the 2nd run; [b] recalculated to the PCL content; [c] ΔH_{ref} = 136.1 J/g[59].

In DSC, melting and crystallization peaks could be observed in the samples containing PCL. It can be seen, from the Table 2, that the grafting of PCL from MWCNT-OH led to a significant increase in the crystallization temperature. This is in good agreement with the previously reported nucleation effect of fillers on PCL crystallization[60]. The increase in T_c is less pronounced for MWCNT-PHEMA-*g*-PCL, which may be due to the covering of the MWCNT surface by PHEMA chains, thus decreasing the nucleation effect. In addition, a similar decrease in T_c was also observed for PHEMA-*g*-PCL, compared to PCL (see Table 2) [61]. Despite the strong nucleation effect of MWCNTs, a lower crystallinity was observed for the PCL grafted on MWCNTs. This may be due to the lower mobility of the grafted PCL chains[60]. In the case

of MWCNT-PHEMA-*g*-PCL, the crystallinity is, however, not so dramatically decreased, compared to the crystallinity of pure PCL. This is in good agreement with the reported observation that both the T_m and crystallinity of grafted PCL increased with the increasing of the grafting density[60]. In MWCNTs-PHEMA-*g*-PCL, the grafting density of PCL can be expected to be higher than for grafted MWCNTs-PCL with a quite low density, as described above. In addition, the crystallinity is closer to that of pure PCL for MWCNT-PHEMA-*g*-PCL hybrids, which may be due to the significantly higher content of PCL, compared to MWCNT-PCL hybrids.

Morphology

First, the MWCNTs modified with the RAFT agent, as well as the MWCNTs grafted with either PCL or PHEMA-*g*-PCL copolymer, were visualized using profilometry (Figure 7). In the case of MWCNTs-CPAD, both individual and small aggregates could be visible. After the surface initiation of the ROP of ε-CL from MWCNTs-OH, it can be clearly seen that some parts of the MWCNTs are not modified, while some bundles are still present, which are paradoxically located at the part where the grafted PCL is presented. Evidently, the PCL is grown only from a few active hydroxyls from the MWCNTs surface. This is in good agreement with the low grafting density calculated from the TGA. Profilometry thus showed a high tendency of MWCNTs-PCL to stack and lower aggregation of CNTs, compared to MWCNTs-CPAD, was not achieved. In the case of MWCNTs-PHEMA-*g*-PCL, the images confirmed the presence of preferably individual MWCNTs evenly coated with a copolymer layer. This observation confirms the effectiveness of the copolymer grafting process in the breaking of MWCNT bundles and improving their dispersion.

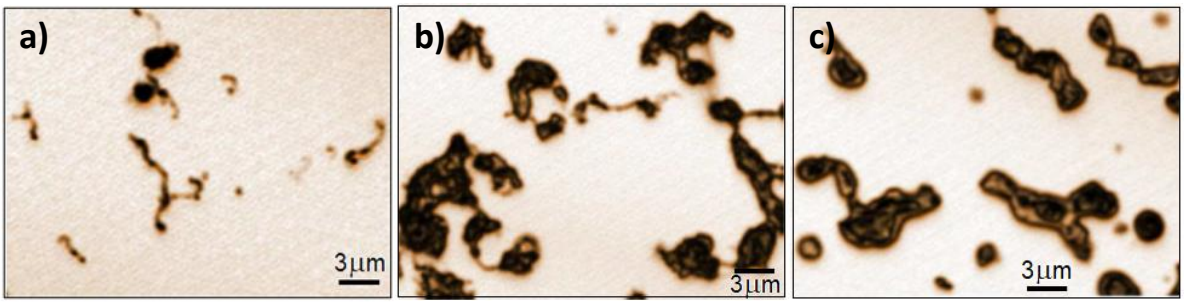

Figure 7. Profilometry of (a) MWCNTs-CPAD, (b) MWCNTs-PCL, and (c) MWCNTs-PHEMA-*g*-PCL.

As for the morphology study, atomic force microscopy (AFM), which is one of the most versatile methods, combining high resolution and surface integrity of samples, was used. Figure 8 shows the height, amplitude, and phase profiles obtained from the MWCNT hybrids. Due to the amorphous nature of PHEMA, the order structure of individual CNTs covered by PHEMA can be observed in the case of the MWCNTs-PHEMA hybrid (Figure 8, left images). Conversely, PCL crystallites[62] forming a symmetrical triangular structure in the case of the MWCNT-PCL hybrids fully suppressed the visibility of CNTs (Figure 8, middle images). In the case of the MWCNT-PHEMA-*g*-PCL hybrids, the PCL did not crystalize in the triangular structures (Figure 8, right images). The reason may be that shorter PCL chains and/or their higher grafting density also affect the size of the PCL crystallites. This is in agreement with the observation from the XRD analysis.

Physical properties of MWCNTs-PHEMA-g-PCL

The conductivity of the MWCNTs-PHEMA-*g*-PCL was measured under an AC field by a frequency sweep. As can be seen in Figure S12, the conductivity of this hybrid was found to be approximately 10^{-5} S cm^{-1}. Considering that the hybrid contains about 24 wt.% of MWCNTs, the conductivity is lower than that described for the PCL composites with even one order of magnitude lower MWCNTs filling[63]. The reason is that the uniform shell of the insulative

polymer in MWCNTs-PHEMA-*g*-PCL serves as an electrical barrier between the MWCNTs cores and prevents conductive pathway formation, which leads to a decrease of the conductivity of the hybrid, even though the MWCNT concentration is high. This is in good agreement with the results described by Hayashida et al. for MWCNTs grafted with poly(cyclohexyl methacrylate)[64], who showed that the conductivity of the hybrid, compared to the composite, both containing 15 wt.% of MWCNTs, was approximately 7 orders lower.

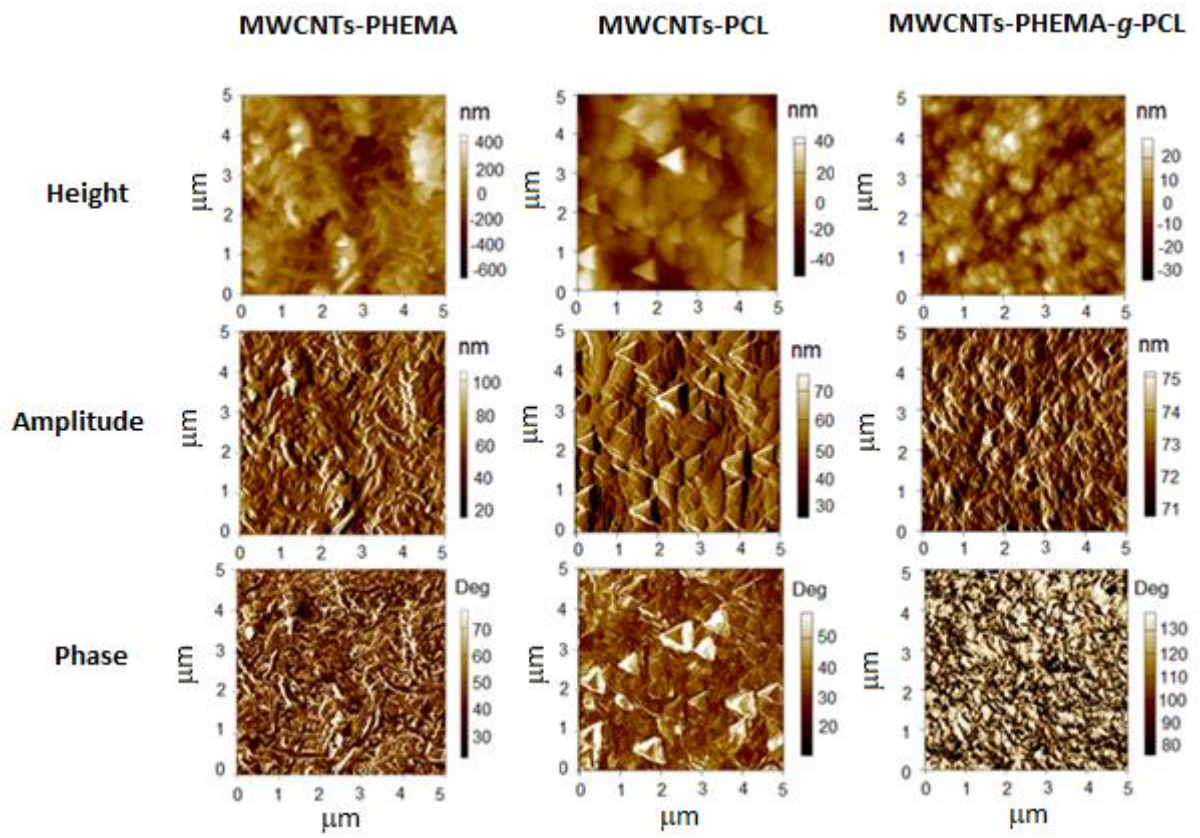

Figure 8. AFM images (height, amplitude, and phase profiles) of MWCNTs grafted with PHEMA, PCL, and PHEMA-*g*-PCL chains.

It should be mentioned that the conductivity of the MWCNT-PHEMA-*g*-PCL hybrids was approximately the same in the whole measured range of frequencies. Conversely, when the conductivity of the poly(divinylbenzene)-coated MWCNT hybrids in epoxy resins was tested,

it linearly increased through several orders with the frequency, almost independently of the hybrid loadings[65].

In order to show the influence of the grafting of MWCNT surfaces on the mechanical performance, the synthesized samples of both the neat PHEMA-*g*-PCL copolymer and MWCNT-PHEMA-*g*-PCL hybrid were analyzed in the dynamic mode, because their intended application is photo-mechanical actuators, where the dynamic deformation prevails. In Figure 9a, it can be seen that the hybrid showed an enhanced deformation, while the constant behavior at 350 kPa for G` was stable almost in the whole range of the investigated strain, only with a negligible decrease at a strain of approximately 1. Thus, no crossing point with G`` due to the transition from solid to liquid-like behavior was observed, unlike in the case of the PHEMA-*g*-PCL copolymer, with a crossing point at a deformation strain of 0.7. This behavior, together with the lower values of both viscoelastic moduli, clearly indicate a better elasticity of the hybrid material. This can be attributed to the presence of a higher amount of smaller crystallites and/or the absence of PCL homopolymer, which could easily be washed out from the hybrids, unlike the PHEMA-*g*-PCL copolymer. It can also be seen, in Figure 9b, that both materials, the neat copolymer and hybrid, show a stable behavior in the investigated range of frequencies, indicating a high potential for real applications.

The dynamic mechanical analysis in the temperature range from 25 to 100°C was further investigated (Figure 10). At 25°C, the neat copolymer showed higher values of storage modulus and lower values of tan delta, indicating that it is a stiffer material. The hybrids exhibited lower values of storage modulus and higher values of tan delta. This could be due to the presence of a large number of small crystallites, which provide a more elastic structure. In addition, while the storage modulus of the copolymer progressively decreases with the temperature over the PCL melting region, an elastic behavior can be observed in the case of the hybrid, showing relatively high and stable values up to 100 °C. Thus, even after the melting of the PCL chains,

the MWCNTs act as crosslink points of the entangled melted polymer chains, ensuring the elasticity of the material. In the photo-actuation systems, the light absorbed by MWCNTs is transformed into heat and released into the surrounding polymer environment. Close to the MWCNTs, however, local overheating can occur, and retaining the elastic behavior of the material at higher temperatures, i.e., at least up to 100 °C, is therefore highly desired.

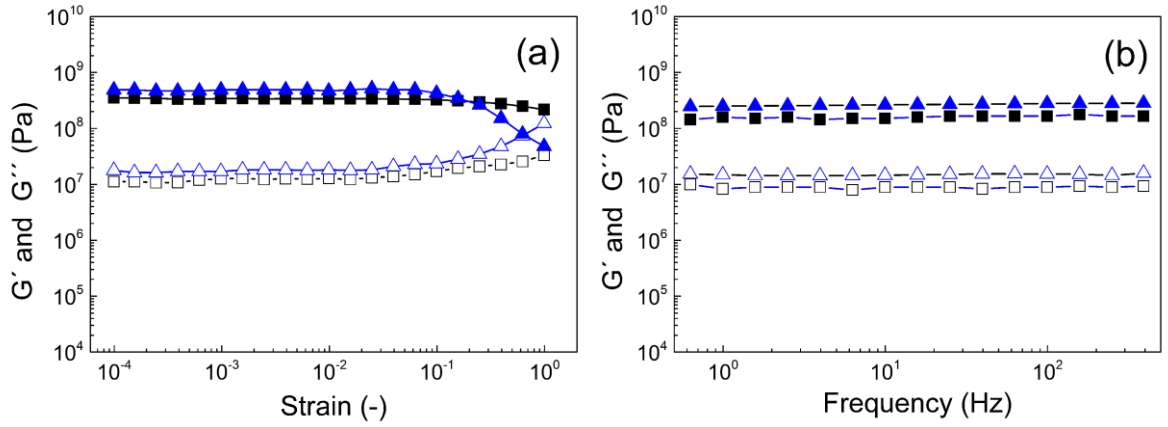

Figure 9. Amplitude (a) and Frequency (b) sweep of the storage moduli (solid symbols) and loss moduli (open symbols) for the neat HEMA-*g*-PCL copolymer (blue triangles) and MWCNT-HEMA-*g*-PCL hybrid (black squares).

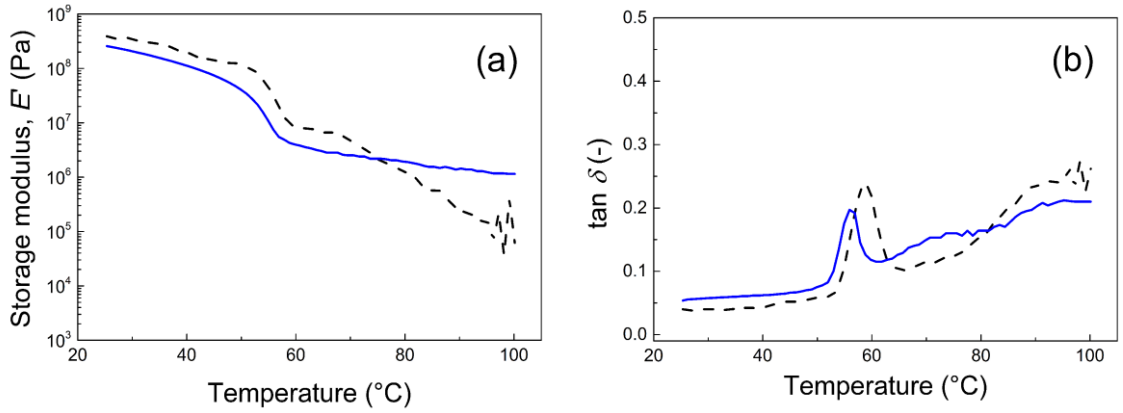

Figure 10. Temperature sweep of the storage modulus *E`* (a) and tan delta (b) for the neat PHEMA-*g*-PCL copolymer (black dashed line) and MWCNTs-PHEMA-*g*-PCL hybrids (blue solid line).

In order to show that the hybrid material acts as a photo-mechanical actuator [66], the typical change in the length of the sample (ΔL) was investigated using a 627 nm wavelength diode as a light source, similar to the process employed in previous works based on composites with graphene oxide [67–69] or CNTs [34,35]. It should be mentioned that the neat PHEMA-*g*-PCL copolymer shows an ΔL of 10 μm (Figure 11), which is a typical value for neat elastic matrices used in photo-mechanical actuation applications (7 μm for neat PDMS [67], or 12 μm for neat Vistamaxx [34]). The performance of the neat MWCNT-PHEMA-*g*-PCL sample under an intensity of light of 6 mW cm^{-2} showed a length change of nearly 50 μm in a 10 s light-on regime and a fully reversible process to the starting length after a 25 s light-off regime (Figure 11). Such behavior of the MWCNT-PHEMA-*g*-PCL sample was fully reversible and repeatable within the investigated 11 consecutive light on-off cycles. Such a length change is significantly higher than that previously reported for composites consisting of MWCNT-based hybrids in styrene-*b*-isoprene-*b*-styrene thermoplastic elastomer, with a reported change rate of 0.4 μm s^{-1} at 5.8 mW cm^{-2}, [34] and it is comparable to those obtained for graphene oxide-based hybrids either in PDMS elastomer (ΔL = 10-75 μm at 6 mW cm^{-2}, depending on the GO concentration and grafted polymer structure) [67,68] or thermoplastic elastomer, such as Vistamaxx (ΔL up to 120 μm at 6 mW cm^{-2}, depending on the GO concentration) [70]. A significantly higher ΔL of 280 μm at 6.6. mW was previously reported only for composites consisting of poly(methyl methacrylate)-*block*-poly(butyl acrylate)-*block*-poly(methyl methacrylate) (PMMA-*b*-PBA-*b*-PMMA) triblock copolymer filled with MWCNTs-PBL-*b*-PMMA hybrids[35]. In that case, however, the baseline was not stable, and both the baseline and signal slightly and progressively decreased with the number of cycles. The reason for this may be the partial interaction of the MWCNT hybrids with a "hard" PMMA phase leading to the deterioration of the physical crosslinking of the system, which is similar to what was described for MWCNTs in SIS composites[71]. Conversely, in the system reported here, both the signal and baseline are stable.

Since there is no matrix presented, and the material consists only of neat MWCNTs hybrids, the MWCNTs can effectively serve as crosslinking points, even if some of the crystalline PCL domains may melt due to the heat formed by the transformation of the light absorbed by the MWCNTs.

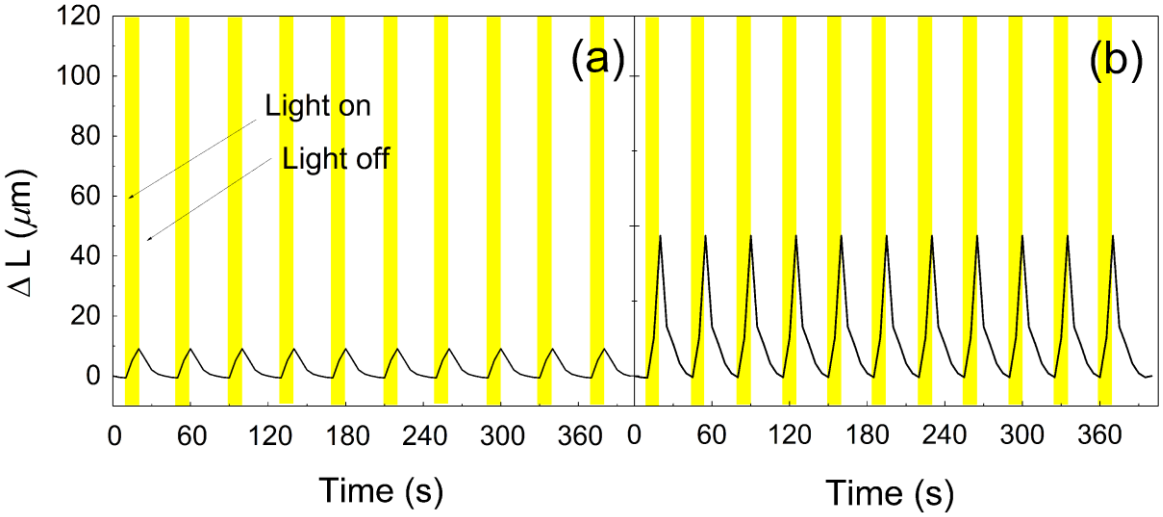

Figure 11. Photoactuation performance after 10s of illumination for the PHEMA-*g*-PCL copolymer (a) and MWCNT-PHEMA-*g*-PCL hybrid (b) at a light power of 6 mW cm^{-2} and ambient temperature in 11 consecutive cycles of illumination in an on (10 s, yellow area) and off (25 s, white area) regime.

The photoactuation performance of MWCNT-PHEMA-*g*-PCL was also investigated at various light intensities. For all of the investigated intensities, a fully reversible process was observed in light on/off cycles, and the changes of the length maxima in the 10s light on regime were 48, 65, and 90 μm for 6, 9, and 12 mW, respectively (Figure 12). Regardless of the light intensity and resultant length change, the time for expansion and contraction was the same and efficient. It is assumed that the hybrid system consisting of MWCNTs with covalently linked PHEMA-*g*-PCL as a polymer shell, prepared in a controlled manner, allows for the homogeneous distribution of the MWCNTs within the material. For this reason, any dramatic

local overheating due to agglomerates is overcome, and the heat energy is homogeneously distributed within the whole material, so the photo-mechanical actuation can be more effective. The very important thing to note here is that the presented system possesses an excellent response and subsequent recovery to the initial state, which is very beneficial and was observed for chemically cross-linked systems based on PDMS[67–69]. The systems based on thermoplastic elastomers have not followed this trend[34] so far. This property has consequences: first, the proper redistribution of the heat formed after light stimulation due to the homogenously dispersed MWCNTs; and secondly, the knowledge that, generally, chemically cross-linked systems showed a better mechanical stability than common physically cross-linked systems, which can show a certain creeping behavior under cyclic deformation when subjected to a mechanical load. As shown in Figure 10, in the current system, the MWCNTs can act as crosslinking points, retaining elastic properties even at a higher temperature and contributing to a good shape recovery. The reproducibility and repeatability of this behavior were confirmed by 11 consecutive cycles for all of the applied intensities. A maximum experiment result of approximately 0.1 mm for 12 mW cm^{-2} can be acceptable and suitable for the intended applications in tactile displays[72] and also play the role of photo-mechanical actuator.

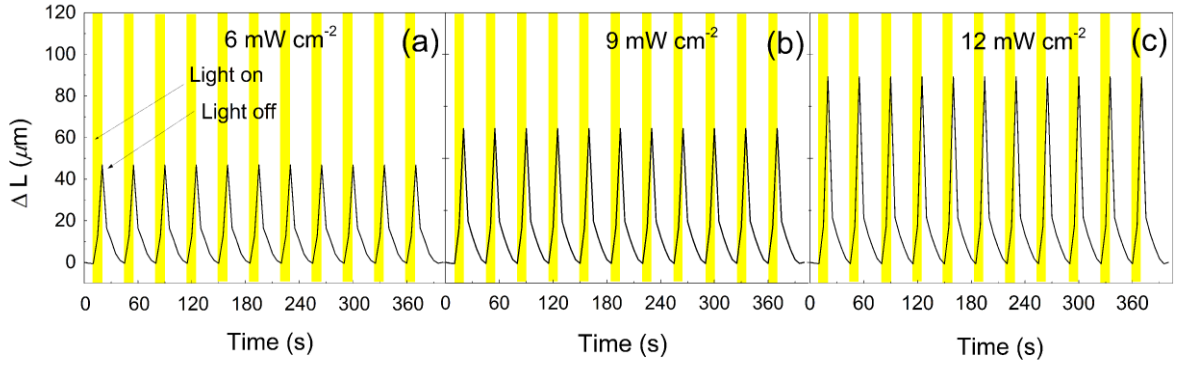

Figure 12. Photoactuation performance for the neat MWCNT-PHEMA-*g*-PCL hybrid at a light power of 6 mW cm^{-2} (a), 9 mW cm^{-2} (b), and 12 mW cm^{-2} (c) at an ambient temperature in 11

consecutive cycles of illumination during an on (10 s, yellow area) and off (25 s, white area) regime.

CONCLUSIONS

The surface of the MWCNTs modified by CPAD as CTA was successfully grafted with the PHEMA-*g*-PCL copolymer by the combination of SI-RAFT and ROP techniques. The synthesized MWCNT-PHEMA-*g*-PCL hybrids contained 24 wt.% of MWCNTs, and the molar ratio of the CL/HEMA units was 46, as calculated from the TGA. The crystallization of the PCL in the MWCNT-PHEMA-*g*-PCL hybrids was affected by both the nucleation effect of MWCNTs and steric hinderance in densely grafted chains, leading to crystallization at higher temperatures and the formation of smaller crystal domains, compared to the pure PCL homopolymer and PHEMA-*g*-PCL copolymer. The investigation of the mechanical properties using viscoelastic measurements showed lower values of storage moduli and higher values of tan delta, indicating a more elastic behavior of the hybrid sample, compared to the PHEMA-*g*-PCL copolymer. This trend was maintained at elevated temperatures, including above the melting temperature of PCL. Such behavior can be connected to the presence of MWCNTs, which act as crosslinking points between the entanglements of melted PCL chains. Importantly, the high photo-mechanical actuation capability of the neat MWCNT-PHEMA-g-PCL hybrid materials was proved, achieving fully reversible and repeatable changes over a sample length of 48 μm and 90 μm for at least 11 consecutive light on-off cycles at 6 mW and 12 mW light intensities, respectively. To the best of our best knowledge, this is the first reported photo-mechanical actuation system based purely on a hybrid material, i.e., without the use of any elastic matrix. The advantage of such a system is that modified MWCNTs with a covalently linked size-controlled PHEMA-*g*-PCL polymer shell are homogeneously, regularly, and uniformly distributed within the material itself. Thus, dramatic local overheating due to

agglomerates is overcome, and the heat energy is homogeneously distributed within the whole material, so the photoactuation can be more effective and efficient. Such an approach opens a pathway for the design of hybrid materials with a controlled architecture for photo-mechanical actuation applications.

In addition, despite the high MWCNT content, the conductivity of the hybrid was found to be only in the order of 10^{-5} Scm^{-1} due to the thick and homogeneous polymer shell, which acted as an insulator. This broadens the potential application of such flexible hybrids, possessing a resistivity in the order of 10^5 Ohm cm, for area of pressure sensors for human body motion[73], indicating a further direction for studies on this material.

ASSOCIATED CONTENT

Supporting Information. ^{1}H NMR, ^{13}C NMR, UV-vis, FTIR, GPC and MALDI-TOF spectra of some copolymers before and after postfunctionalization. This material is available free of charge via the Internet at http://pubs.acs.org.

AUTHOR INFORMATION

Corresponding Authors

E-mail: katarina.mosnackova@savba.sk (K. Mosnáčková); peter.kasak@qu.edu.qa (P. Kasák); jaroslav.mosnacek@savba.sk (J. Mosnáček)

Author Contributions

The manuscript was written through contributions of all authors. All authors have given approval to the final version of the manuscript. The authors declare no competing financial interest.

ACKNOWLEDGEMENTS

The authors express their gratitude for the financial support associated with projects VEGA 2/0019/18, APVV 18-0420, APVV-19-0338, and SAS-MOST JRP 2019/07. K.M. also gratefully acknowledges the financial support of the Slovak Academic Information Agency within the "Action Austria – Slovakia" program. M.M. would like to acknowledge the financial support of the Ministry of Education, Youth and Sports of the Czech Republic - DKRVO (RP/CPS/2020/003). This study was also performed during the implementation of the project Building-up Centre for advanced materials application of the Slovak Academy of Sciences, ITMS project code 313021T081 supported by Research & Innovation Operational Programme funded by the ERDF. P.K. thanks for fund through the Qatar University Collaborative Grant No. QUCG-CAM 19/20-3. The findings achieved herein are solely the responsibility of the authors.

REFERENCES

(1) Iijima, S. Helical Microtubules of Graphitic Carbon. *Nature* **1991**, *354*, 56–58.

(2) Dyke, C. A.; Tour, J. M. Overcoming the Insolubility of Carbon Nanotubes through High Degrees of Sidewall Functionalization. *Chem. - A Eur. J.* **2004**, *10* (4), 812–817. https://doi.org/10.1002/chem.200305534.

(3) Zhao, X.-D.; Fan, X.-H.; Chen, X.-F.; Chai, C.-P.; Zhou, Q.-F. Surface Modification of Multiwalled Carbon Nanotubes via Nitroxide-Mediated Radical Polymerization. *J. Polym. Sci. Part A Polym. Chem.* **2006**, *44* (15), 4656–4667. https://doi.org/10.1002/pola.21570.

(4) Roghani-Mamaqani, H.; Haddadi-Asl, V.; Ghaderi-Ghahfarrokhi, M.; Sobhkhiz, Z. Reverse Atom Transfer Radical Polymerization of Methyl Methacrylate in the Presence of Azo-Functionalized Carbon Nanotubes: A Grafting from Approach. *Colloid Polym. Sci.* **2014**, *292*, 2971–2981. https://doi.org/10.1007/s00396-014-3349-y.

(5) Atif, R.; Inam, F. Reasons and Remedies for the Agglomeration of Multilayered Graphene and Carbon Nanotubes in Polymers. *Beilstein J. Nanotechnol.* **2016**, *7* (1), 1174–1196. https://doi.org/10.3762/bjnano.7.109.

(6) Gofman, I. V.; Abalov, I. V.; Vlasova, E. N.; Goikhman, M. J.; Zhang, B. Comparative Evaluation of Different Methods of Carboxylation of Carbon Nanotubes as a Modifier of Mechanical Properties of Heat-Resistant Polyimide Based Nanocomposites. *Fibre Chem.* **2015**, *47* (4), 236–243. https://doi.org/10.1007/s10692-016-9671-z.

(7) Xu, G.; Wu, W.-T.; Wang, Y.; Pang, W.; Zhu, Q.; Wang, P.; You, Y. Constructing Polymer Brushes on Multiwalled Carbon Nanotubes by in Situ Reversible Addition Fragmentation Chain Transfer Polymerization. *Polymer (Guildf).* **2006**, *47* (16), 5909–5918. https://doi.org/10.1016/j.polymer.2006.06.027.

(8) Zhang, B.; Wang, J.; Chen, Y.; Früchtl, D.; Yu, B.; Zhuang, X.; He, N.; Blau, W. J. Multiwalled Carbon Nanotubes Covalently Functionalized with Poly(N-Vinylcarbazole) via RAFT Polymerization: Synthesis and Nonliner Optical Properties. *J. Polym. Sci. Part A Polym. Chem.* **2010**, *48* (14), 3161–3168. https://doi.org/10.1002/pola.24099.

(9) Yang, Q.; Wang, L.; Xiang, W.; Zhou, J.; Tan, Q. hua. A Temperature-Responsive Carbon Black Nanoparticle Prepared by Surface-Induced Reversible Addition-Fragmentation Chain Transfer Polymerization. *Polymer (Guildf).* **2007**, *48* (12), 3444–3451. https://doi.org/10.1016/j.polymer.2007.02.064.

(10) Pei, X.; Hao, J.; Liu, W. Preparation and Characterization of Carbon Nanotubes-Polymer / Ag Hybrid Nanocomposites via Surface RAFT Polymerization. *J. Phys. Chem. C* **2007**, *111*, 2947–2952. https://doi.org/10.1021/jp0673213.

(11) Lipińska, M. E.; Rebelo, S. L. H.; Pereira, M. F. R.; Gomes, J. A. N. F.; Freire, C.; Figueiredo, J. L. New Insights into the Functionalization of Multi-Walled Carbon Nanotubes

with Aniline Derivatives. *Carbon N. Y.* **2012**, *50* (9), 3280–3294. https://doi.org/10.1016/j.carbon.2011.12.018.

(12) Buffa, F.; Hu, H. and; Resasco, D. E. Side-Wall Functionalization of Single-Walled Carbon Nanotubes with 4-Hydroxymethylaniline Followed by Polymerization of ε-Caprolactone. *Macromolecules* **2005**, *38* (20), 8258–8263. https://doi.org/10.1021/MA050876W.

(13) Brzeziński, M.; Bogusławska, M.; Ilčíková, M.; Mosnáček, J.; Biela, T. Unusual Thermal Properties of Polylactides and Polylactide Stereocomplexes Containing Polylactide-Functionalized Multi-Walled Carbon Nanotubes. *Macromolecules* **2012**, *45* (21), 8714–8721. https://doi.org/10.1021/ma301554q.

(14) Wu, W.; Tsarevsky, N. V.; Hudson, J. L.; Tour, J. M.; Matyjaszewski, K.; Kowalewski, T. "Hairy" Single-Walled Carbon Nanotubes Prepared by Atom Transfer Radical Polymerization. *Small* **2007**, *3* (10), 1803–1810. https://doi.org/10.1002/smll.200600688.

(15) Mosnáčková, K.; Kollár, J.; Huang, Y.-S.; Huang, C.-F.; Mosnáček, J. *Polymer Composites with Functionalized Nanoparticles : Synthesis, Properties, and Applications. Synthesis Routes of Functionalized Nanoparticles.*; Pielichowski, K., Majka, T. M., Eds.; 2019.

(16) Li, Y.; Benicewicz, B. C. Functionalization of Silica Nanoparticles via the Combination of Surface-Initiated RAFT Polymerization and Click Reactions Functionalization of Silica Nanoparticles via the Combination of Surface-Initiated RAFT Polymerization and Click Reactions. *Macromolecules* **2008**, *41*, 7986–7992. https://doi.org/10.1021/ma801551z.

(17) Vega-Rios, A.; Licea-Claveríe, A. Controlled Synthesis of Block Copolymers Containing N-Isopropylacrylamide by Reversible Addition-Fragmentation Chain-Transfer (RAFT) Polymerization. *J. Mex. Chem. Soc* **2011**, *55* (1), 21–32. https://doi.org/ISSN 1870-249X.

(18) Gregory, A.; Stenzel, M. H. Complex Polymer Architectures via RAFT Polymerization: From Fundamental Process to Extending the Scope Using Click Chemistry and Nature's Building Blocks. *Prog. Polym. Sci.* **2012**, *37* (1), 38–105. https://doi.org/10.1016/j.progpolymsci.2011.08.004.

(19) McKenzie, T. G.; Fu, Q.; Uchiyama, M.; Satoh, K.; Xu, J.; Boyer, C.; Kamigaito, M.; Qiao, G. G. Beyond Traditional RAFT: Alternative Activation of Thiocarbonylthio Compounds for Controlled Polymerization. *Adv. Sci. (Weinheim, Baden-Wurttemberg, Ger.* **2016**, *3* (9), 1500394. https://doi.org/10.1002/advs.201500394.

(20) Rotzoll, R.; Vana, P. A Bipedal Silica-Immobilized Azo-Initiator for Surface-Confined Radical Polymerizations. *Aust. J. Chem.* **2009**, *62* (11), 1473–1478. https://doi.org/10.1071/CH09189.

(21) Baum, M.; Brittain, W. J. Synthesis of Polymer Brushes on Silicate Substrates via Reversible Addition Fragmentation Chain Transfer Technique. *Macromolecules* **2002**, *35* (3), 610–615. https://doi.org/10.1021/MA0112467.

(22) Moraes, J.; Ohno, K.; Maschmeyer, T.; Perrier, S. Synthesis of Silica–Polymer Core–Shell Nanoparticles by Reversible Addition–Fragmentation Chain Transfer Polymerization. *Chem. Commun.* **2013**, *49* (80), 9077–9088. https://doi.org/10.1039/c3cc45319g.

(23) Perrier, S.; Takolpuckdee, P.; Mars, C. A. Reversible Addition−Fragmentation Chain Transfer Polymerization Mediated by a Solid Supported Chain Transfer Agent. *Macromolecules* **2005**, *38* (16), 6770–6774. https://doi.org/10.1021/ma0506886.

(24) Yang, Q.; Wang, L.; Xiang, W.; Zhou, J.; Deng, L.; Li, J. Preparation of Core-Shell Carbon Black Nanoparticles and Their Crystallization-Induced Orientation. *Eur. Polym. J.* **2007**, *43* (5), 1718–1723. https://doi.org/10.1016/j.eurpolymj.2006.11.035.

(25) Cao, X. T.; Showkat, A. M.; Park, C.; Gal, Y. S.; Lim, K. T. Synthesis of Poly(ϵ-Caprolactone) Grafted Poly(2-Hydroxyethyl Methacrylate) Functionalized Hydroxyapatite by RAFT and ROP. *Mol. Cryst. Liq. Cryst.* **2015**, *618* (1), 103–110. https://doi.org/10.1080/15421406.2015.1076299.

(26) Hong, C.-Y.; You, Y.-Z.; Pan, C.-Y. Synthesis of Water-Soluble Multiwalled Carbon Nanotubes with Grafted Temperature-Responsive Shells by Surface RAFT Polymerization. *Chem. Mater.* **2005**, *17* (9), 2247–2254. https://doi.org/10.1021/cm048054l.

(27) Stenzel, M. H.; Zhang, L.; Huck, W. T. S. Temperature-Responsive Glycopolymer Brushes Synthesized via RAFT Polymerization Using the Z-Group Approach. *Macromol. Rapid Commun.* **2006**, *27* (14), 1121–1126. https://doi.org/10.1002/marc.200600223.

(28) Nguyen, D. H.; Vana, P. Silica-Immobilized Cumyl Dithiobenzoate as Mediating Agent in Reversible Addition Fragmentation Chain Transfer (RAFT) Polymerization. *Polym. Adv. Technol.* **2006**, *17* (9–10), 625–633. https://doi.org/10.1002/pat.826.

(29) Zhao, Y.; Perrier*, S. Synthesis of Well-Defined Homopolymer and Diblock Copolymer Grafted onto Silica Particles by Z-Supported RAFT Polymerization. *Macromolecules* **2006**, *39* (25), 8603–8608. https://doi.org/10.1021/MA061586Y.

(30) Zhang, X.; Yu, Z.; Wang, C.; Zarrouk, D.; Seo, J. W. T.; Cheng, J. C.; Buchan, A. D.; Takei, K.; Zhao, Y.; Ager, J. W.; Zhang, J.; Hettick, M.; Hersam, M. C.; Pisano, A. P.; Fearing, R. S.; Javey, A. Photoactuators and Motors Based on Carbon Nanotubes with Selective Chirality Distributions. *Nat. Commun.* **2014**, *5* (1), 1–8. https://doi.org/10.1038/ncomms3983.

(31) Ilčíková, M.; Mrlík, M.; Sedláček, T.; Doroshenko, M.; Koynov, K.; Danko, M.; Mosnáček, J. Tailoring of Viscoelastic Properties and Light-Induced Actuation Performance of Triblock Copolymer Composites through Surface Modification of Carbon Nanotubes. *Polymer (Guildf).* **2015**, *72*, 368–377. https://doi.org/10.1016/J.POLYMER.2015.03.060.

(32) Ji, Y.; Huang, Y. Y.; Rungsawang, R.; Terentjev, E. M. Dispersion and Alignment of Carbon Nanotubes in Liquid Crystalline Polymers and Elastomers. *Adv. Mater.* **2010**, *22* (31), 3436–3440. https://doi.org/10.1002/adma.200904103.

(33) Czaniková, K.; Torras, N.; Esteve, J.; Krupa, I.; Kasák, P.; Pavlova, E.; Račko, D.; Chodák, I.; Omastová, M. Nanocomposite Photoactuators Based on an Ethylene Vinyl Acetate Copolymer Filled with Carbon Nanotubes. *Sensors Actuators, B Chem.* **2013**, *186*, 701–710. https://doi.org/10.1016/j.snb.2013.06.054.

(34) Ilčíková, M.; Mrlík, M.; Sedláček, T.; Chorvát, D.; Krupa, I.; Šlouf, M.; Koynov, K.; Mosnáček, J. Viscoelastic and Photo-Actuation Studies of Composites Based on Polystyrene-Grafted Carbon Nanotubes and Styrene-b-Isoprene-b-Styrene Block Copolymer. *Polymer (Guildf).* **2014**, *55* (1), 211–218. https://doi.org/10.1016/J.POLYMER.2013.11.031.

(35) Ilčíková, M.; Mrlík, M.; Sedláček, T.; Šlouf, M.; Zhigunov, A.; Koynov, K.; Mosnáček, J. Synthesis of Photoactuating Acrylic Thermoplastic Elastomers Containing Diblock Copolymer-Grafted Carbon Nanotubes. *ACS Macro Lett.* **2014**, *3* (10), 999–1003. https://doi.org/10.1021/mz500444m.

(36) XRD Crystallite Size Calculator (Scherrer Equation) | InstaNANO https://www.instanano.com/2017/01/xrd-crystallite-size-calculator-scherrer-equation.html (accessed Aug 20, 2020).

(37) Tang, B.; Wang, Y.; Qiu, M.; Zhang, S. A Full-Band Sunlight-Driven Carbon Nanotube/PEG/SiO2 Composites for Solar Energy Storage. *Sol. Energy Mater. Sol. Cells* **2014**, *123*, 7–12. https://doi.org/10.1016/j.solmat.2013.12.022.

(38) Moad, G. Mechanism and Kinetics of Dithiobenzoate-Mediated RAFT Polymerization - Status of the Dilemma. *Macromol. Chem. Phys.* **2014**, *215* (1), 9–26. https://doi.org/10.1002/macp.201300562.

(39) Lee, J. M.; Kim, O. H.; Shim, S. E.; Lee, B. H.; Choe, S. Reversible Addition-Fragmentation Chain Transfer (RAFT) Bulk Polymerization of Styrene : Effect of R-Group Structures of Carboxyl Acid Group Functionalized RAFT Agents. *Macromol. Res.* **2005**, *13* (3), 236–242. https://doi.org/10.1007/BF03219058.

(40) Chernikova, E. V.; Zaitsev, S. D.; Plutalova, A. V.; Mineeva, K. O.; Zotova, O. S.; Vishnevetsky, D. V. Control over the Relative Reactivities of Monomers in RAFT Copolymerization of Styrene and Acrylic Acid. *RSC Adv.* **2018**, *8* (26), 14300–14310. https://doi.org/10.1039/C8RA00048D.

(41) Luo, S.; Xu, J.; Zhang, Y.; Liu, S.; Wu, C. Double Hydrophilic Block Copolymer Monolayer Protected Hybrid Gold Nanoparticles and Their Shell Cross-Linking. *J. Phys. Chem. B* **2005**, *109* (47), 22159–22166. https://doi.org/10.1021/jp0549935.

(42) Yuan, J.; Huang, X.; Li, P.; Li, L.; Shen, J. Surface-Initiated RAFT Polymerization of Sulfobetaine from Cellulose Membranes to Improve Hemocompatibility and Antibiofouling Property. *Polym. Chem.* **2013**, *4* (19), 5074. https://doi.org/10.1039/c3py00565h.

(43) Chen, Y.; Gan, T.; Ma, C.; Wang, L.; Zhang, G. Crystallization of Polymer Chains Chemically Attached on a Surface: Lamellar Orientation from Flat-on to Edge-On. *J. Phys. Chem. B* **2016**, *120* (20), 4715–4722. https://doi.org/10.1021/acs.jpcb.6b02344.

(44) Yuan, W.; Yuan, J.; Zhou, L.; Wu, S.; Hong, X. Fe3O4@poly(2-Hydroxyethyl Methacrylate)-Graft-Poly(ε-Caprolactone) Magnetic Nanoparticles with Branched Brush Polymeric Shell. *Polymer (Guildf).* **2010**, *51* (12), 2540–2547. https://doi.org/10.1016/j.polymer.2010.04.016.

(45) Yang, Q.; Wang, L.; Huo, J.; Ding, J.; Xiang, W. Novel Comb-Structured-Polymer-Grafted Carbon Black by Surface-Initiated Atom Transfer Radical Polymerization and Ring-Opening Polymerization. *J. Appl. Polym. Sci.* **2010**, *117* (2), 824–827.

https://doi.org/10.1002/app.31142.

(46) Cheng, R.; Wang, X.; Chen, W.; Meng, F.; Deng, C.; Liu, H.; Zhong, Z. Biodegradable Poly(ε-Caprolactone)-g-Poly(2-Hydroxyethyl Methacrylate) Graft Copolymer Micelles as Superior Nano-Carriers for "Smart" Doxorubicin Release. *J. Mater. Chem.* **2012**, *22* (23), 11730. https://doi.org/10.1039/c2jm30700f.

(47) Atzet, S.; Curtin, S.; Trinh, P.; Bryant, S.; Ratner, B. Degradable Poly(2-Hydroxyethyl Methacrylate)- *Co* -Polycaprolactone Hydrogels for Tissue Engineering Scaffolds. *Biomacromolecules* **2008**, *9* (12), 3370–3377. https://doi.org/10.1021/bm800686h.

(48) ThermoFisher Scientific XPS: Knowledge Base Avantage software 5.9918 https://xpssimplified.com/periodictable.php (accessed Feb 28, 2020).

(49) Hantsche, H. High Resolution XPS of Organic Polymers, the Scienta ESCA300 Database. By G. Beamson and D. Briggs, Wiley, Chichester 1992, 295 Pp., Hardcover, £ 65.00, ISBN 0-471-93592-1. *Adv. Mater.* **1993**, *5* (10), 778–778. https://doi.org/10.1002/adma.19930051035.

(50) Li, C.; Benicewicz*, B. C. Synthesis of Well-Defined Polymer Brushes Grafted onto Silica Nanoparticles via Surface Reversible Addition−Fragmentation Chain Transfer Polymerization. *Macromolecules* **2005**, *38* (14), 5929–5936. https://doi.org/10.1021/MA050216R.

(51) Tsujii, Y.; Ohno, K.; Yamamoto, S.; Goto, A.; Fukuda, T. Structure and Properties of High-Density Polymer Brushes Prepared by Surface-Initiated Living Radical Polymerization; Springer Berlin Heidelberg, 2006; pp 1–45. https://doi.org/10.1007/12_063.

(52) Semsarilar, M.; Perrier, S. "Green" Reversible Addition-Fragmentation Chain-Transfer (RAFT) Polymerization. *Nat. Chem.* **2010**, *2* (10), 811–820.

https://doi.org/10.1038/nchem.853.

(53) Lee, R. S.; Chen, W. H.; Lin, J. H. Polymer-Grafted Multi-Walled Carbon Nanotubes through Surface-Initiated Ring-Opening Polymerization and Click Reaction. *Polymer (Guildf).* **2011**, *52* (10), 2180–2188. https://doi.org/10.1016/j.polymer.2011.03.020.

(54) Niu, L.; Luo, Y.; Li, Z. A Highly Selective Chemical Gas Sensor Based on Functionalization of Multi-Walled Carbon Nanotubes with Poly(Ethylene Glycol). *Sensors Actuators B Chem.* **2007**, *126* (2), 361–367. https://doi.org/10.1016/j.snb.2007.03.018.

(55) Khabashesku, V. N.; Pulikkathara, M. X. Chemical Modification of Carbon Nanotubes. *Mendeleev Commun.* **2006**, *16* (2), 61–66. https://doi.org/10.1070/MC2006V016N02ABEH002316.

(56) Malikov, E. Y.; Muradov, M. B.; Akperov, O. H.; Eyvazova, G. M.; Puskás, R.; Madarász, D.; Nagy, L.; Kukovecz, Á.; Kónya, Z. Synthesis and Characterization of Polyvinyl Alcohol Based Multiwalled Carbon Nanotube Nanocomposites. *Phys. E Low-Dimensional Syst. Nanostructures* **2014**, *61*, 129–134. https://doi.org/10.1016/j.physe.2014.03.026.

(57) Ma, W.; Zhao, Y.; Zhu, Z.; Guo, L.; Cao, Z.; Xia, Y.; Yang, H.; Gong, F.; Zhong, J. Synthesis of Poly(Methyl Methacrylate) Grafted Multiwalled Carbon Nanotubes via a Combination of RAFT and Alkyne-Azide Click Reaction. *Appl. Sci.* **2019**, *9* (3), 603. https://doi.org/10.3390/app9030603.

(58) Ramoraswi, N. O.; Ndungu, P. G. Photo-Catalytic Properties of TiO2 Supported on MWCNTs, SBA-15 and Silica-Coated MWCNTs Nanocomposites. *Nanoscale Res. Lett.* **2015**, *10* (1), 427. https://doi.org/10.1186/s11671-015-1137-3.

(59) Yam, W. Y.; Ismail, J.; Kammer, H. W.; Schmidt, H.; Kummerlöwe, C. Polymer Blends of Poly(ε-Caprolactone) and Poly(Vinyl Methyl Ether) - Thermal Properties and Morphology.

Polymer (Guildf). **1999**, *40* (20), 5545–5552. https://doi.org/10.1016/S0032-3861(98)00807-6.

(60) Zhou, B.; Tong, Z. Z.; Huang, J.; Xu, J. T.; Fan, Z. Q. Isothermal Crystallization Kinetics of Multi-Walled Carbon Nanotubes-Graft-Poly(ε-Caprolactone) with High Grafting Degrees. *CrystEngComm* **2013**, *15* (38), 7824–7832. https://doi.org/10.1039/c3ce40606g.

(61) Yuan, W.; Yuan, J.; Zhang, F.; Xie, X.; Pan, C. Synthesis, Characterization, Crystalline Morphologies, and Hydrophilicity of Brush Copolymers with Double Crystallizable Side Chains. *Macromolecules* **2007**, *40* (25), 9094–9102. https://doi.org/10.1021/ma071841u.

(62) Marrese, M.; Guarino, V.; Ambrosio, L. Atomic Force Microscopy: A Powerful Tool to Address Scaffold Design in Tissue Engineering. *J. Funct. Biomater.* **2017**, *8* (1), 7. https://doi.org/10.3390/jfb8010007.

(63) Wurm, A.; Lellinger, D.; Minakov, A. A.; Skipa, T.; Pötschke, P.; Nicula, R.; Alig, I.; Schick, C. Crystallization of Poly(ε-Caprolactone)/MWCNT Composites: A Combined SAXS/WAXS, Electrical and Thermal Conductivity Study. *Polymer (Guildf).* **2014**, *55* (9), 2220–2232. https://doi.org/10.1016/j.polymer.2014.02.069.

(64) Hayashida, K.; Tanaka, H. Ultrahigh Electrical Resistance of Poly(Cyclohexyl Methacrylate)/Carbon Nanotube Composites Prepared Using Surface-Initiated Polymerization. *Adv. Funct. Mater.* **2012**, *22* (11), 2338–2344. https://doi.org/10.1002/adfm.201103089.

(65) Su, Y.; Ren, Y.; Chen, G. X.; Li, Q. Fabrication of High-: K Epoxy Composites with Low Dielectric Loss Based on Polymer Shell-Coated Multiwalled Carbon Nanotubes. *RSC Adv.* **2016**, *6* (59), 53867–53872. https://doi.org/10.1039/c6ra07945h.

(66) Leeladhar; Raturi, P.; Singh, J. P. Sunlight-Driven Eco-Friendly Smart Curtain Based on Infrared Responsive Graphene Oxide-Polymer Photoactuators. *Sci. Rep.* **2018**, *8* (1), 1–9. https://doi.org/10.1038/s41598-018-21871-3.

(67) Osicka, J.; Mrlik, M.; Ilčíková, M.; Munster, L.; Bazant, P.; Špitalský, Z.; Mosnáček, J. Light-Induced Actuation of Poly(Dimethylsiloxane) Filled with Graphene Oxide Grafted with Poly(2-(Trimethylsilyloxy)Ethyl Methacrylate). *Polymers (Basel).* **2018**, *10* (10). https://doi.org/10.3390/polym10101059.

(68) Osicka, J.; Mrlik, M.; Ilcikova, M.; Hanulikova, B.; Urbanek, P.; Sedlacik, M.; Mosnacek, J. Reversible Actuation Ability upon Light Stimulation of the Smart Systems with Controllably Grafted Graphene Oxide with Poly (Glycidyl Methacrylate) and PDMS Elastomer: Effect of Compatibility and Graphene Oxide Reduction on the Photo-Actuation Performance. *Polymers (Basel).* **2018**, *10* (8). https://doi.org/10.3390/polym10080832.

(69) Osicka, J.; Ilčíková, M.; Mrlik, M.; Minarík, A.; Pavlinek, V.; Mosnácek, J. The Impact of Polymer Grafting from a Graphene Oxide Surface on Its Compatibility with a PDMS Matrix and the Light-Induced Actuation of the Composites. *Polymers (Basel).* **2017**, *9* (7). https://doi.org/10.3390/polym9070264.

(70) Osicka, J.; Mrlik, M.; Ilcikova, M.; Krupa, I.; Sobolčiak, P.; Plachý, T.; Mosnáček, J. Controllably Coated Graphene Oxide Particles with Enhanced Compatibility with Poly(Ethylene-Co-Propylene) Thermoplastic Elastomer for Excellent Photo-Mechanical Actuation Capability. *React. Funct. Polym.* **2020**, *148*, 104487. https://doi.org/10.1016/j.reactfunctpolym.2020.104487.

(71) Ilčíková, M.; Mosnáček, J.; Mrlík, M.; Sedláček, T.; Csomorová, K.; Czaniková, K.; Krupa, I. Influence of Surface Modification of Carbon Nanotubes on Interactions with Polystyrene- *b* -Polyisoprene- *b* -Polystyrene Matrix and Its Photo-Actuation Properties. *Polym. Adv. Technol.* **2014**, *25* (11), 1293–1300. https://doi.org/10.1002/pat.3324.

(72) Torras, N.; Zinoviev, K. E.; Camargo, C. J.; Campo, E. M.; Campanella, H.; Esteve, J.; Marshall, J. E.; Terentjev, E. M.; Omastová, M.; Krupa, I.; Teplický, P.; Mamojka, B.; Bruns,

P.; Roeder, B.; Vallribera, M.; Malet, R.; Zuffanelli, S.; Soler, V.; Roig, J.; Walker, N.; Wenn, D.; Vossen, F.; Crompvoets, F. M. H. Tactile Device Based on Opto-Mechanical Actuation of Liquid Crystal Elastomers. *Sensors Actuators, A Phys.* **2014**, *208*, 104–112. https://doi.org/10.1016/j.sna.2014.01.012.

(73) Tolvanen, J.; Kilpijärvi, J.; Pitkänen, O.; Hannu, J.; Jantunen, H. Stretchable Sensors with Tunability and Single Stimuli-Responsiveness through Resistivity Switching under Compressive Stress. *ACS Appl. Mater. Interfaces* **2020**, *12* (12), 14433–14442. https://doi.org/10.1021/acsami.0c00023.